Postmidnight convection dynamics during substorm expansion phase

Jun Liang,[1,2] G. J. Sofko,[1] and H. U. Frey[3]

Received 18 October 2005; revised 14 December 2005; accepted 10 January 2006; published 7 April 2006.

[1] A study of the dynamics of ionospheric plasma convection in the postmidnight sector during the substorm expansion phase (EP) is presented. We have found that after the substorm onset, a postmidnight anticlockwise convection vortex (PoACV) usually emerges at latitudes higher than the auroral brightening region, and an east-to-west flow reversal wrapping around the intensified auroras extends into the postmidnight sector. The substorm current system inferred from the relative positions of the PoACV and the auroral brightening region is in general northeast-southwest aligned, implying a mixture of a meridional current system (MCS) and a zonal system associated with the substorm current wedge (SCW). The time delay between the formation of the PoACV and the onset depends upon the relative azimuthal location of the PoACV and the auroral brightening region. The observed postmidnight convection pattern, namely, a PoACV at higher latitudes, and an east-to-west flow reversal region at lower latitudes, can be explained by a combination of the nightside reconnection and the "field line slippage" process associated with dipolarization. Finally, we suggest that strong negative IMF By is the most unfavorable condition for the evolution of the PoACV.

Citation: Liang, J., G. J. Sofko, and H. U. Frey (2006), Postmidnight convection dynamics during substorm expansion phase, *J. Geophys. Res.*, *111*, A04205, doi:10.1029/2005JA011483.

1. Introduction

[2] High-latitude ionospheric plasma convection flows usually undergo dramatic changes and display fundamentally different features during successive stages of a magnetospheric substorm. The interaction between the substorm process and the plasma convection has been a topic of rich research interest, aided in part by the convection measurements from the near-global deployment of HF radars in the SuperDARN (Super Dual Auroral Radar Network) program. In a majority of substorms the expansion phase (EP) onset and the most spectacular auroral brightening initiate in the evening and midnight sector [e.g., *Liou et al.*, 2001; *Frey et al.*, 2004]. It has been postulated that during a substorm EP the brightening aurora may act as an obstacle to the flows. Fast flows are diverted around the aurora, while inside the aurora the flows are usually strongly suppressed [*Opgenoorth and Pellinen*, 1998; *Yeoman et al.*, 2000; *Khan et al.*, 2001]. However, the very dynamic substorm EP process may also cause a prompt change in the convection and current system in the postmidnight sector. For example, *Opgenoorth and Pellinen* [1998] presented evidence that flow enhancements in the evening auroral zone soon after the EP onset led to an immediate increase in the global current system. It has also been suggested that during a substorm the nightside reconnection will generate a twin-vortex flow pattern with foci located at both ends of the merging gap, one in the premidnight and the other in the postmidnight sector [*Cowley and Lockwood*, 1992; *Grocott et al.*, 2002].

[3] By using the AMIE (Assimilative Mapping of Ionospheric Electrodynamic) algorithm, *Kamide et al.* [1994, hereinafter referred to as KY94] first proposed that a new pair of convection vortices appears in the nightside during a substorm EP in addition to the preexisting global 2-cell pattern. The new pair of vortices consists of a higher-latitude anticlockwise vortex located mainly in the postmidnight sector, and a lower-latitude clockwise vortex extending from the premidnight to the postmidnight sector. A schematic diagram of the KY94 model is shown in Figure 1. This model was further confirmed through a statistical study of high-latitude ionospheric convection and current patterns during different substorm phases by *Kamide et al.* [1996]. *Kamide and Kokubun* [1996] suggested that these vortices are signatures of the "unloading" component of the auroral electrojet associated with substorm expansion, as opposed to the solar wind "directly driven" component.

[4] One of the most important features of the KY94 model is that the current pattern associated with the two new vortices is characterized by a distinguishable meridional current system (MCS) as opposed to the more azimuthally aligned (zonal) system usually related to the substorm current wedge (SCW) geometry [e.g., *McPherron et al.*, 1973]. *Kamide* [1996] first suggested that the east-west ionospheric closure of the substorm current was overemphasized by most substorm researchers. *Akasofu* [2003] suggested that the substorm current system was initially

[1]Institute of Space and Atmospheric Studies, Department of Physics and Engineering Physics, University of Saskatchewan, Saskatoon, Saskatchewan, Canada.
[2]Now at Canadian Space Agency, Saint-Hubert, Québec, Canada.
[3]Space Sciences Laboratory, University of California, Berkeley, Berkeley, California, USA.

0148-0227/06/2005JA011483$09.00

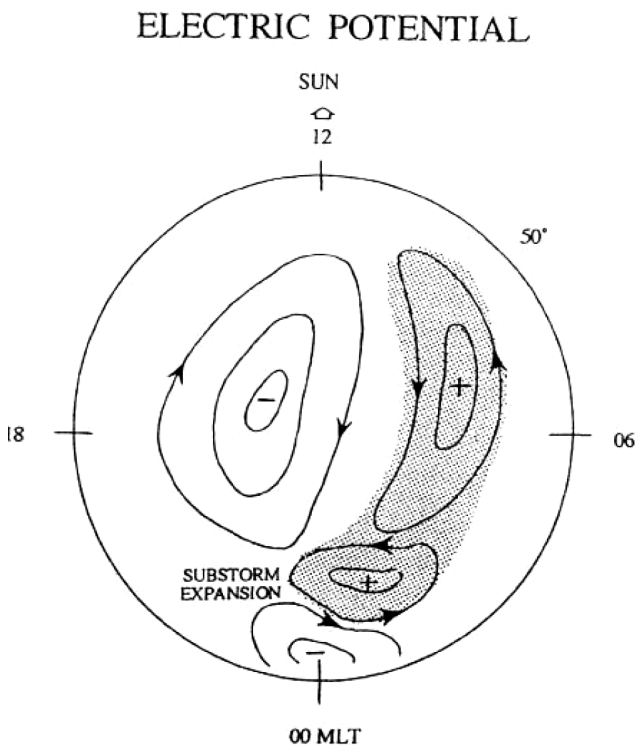

Figure 1. Schematic diagram showing two pairs of electric potential cells, representing the effects of enhanced plasma convection and of the substorm EP. The plus and minus symbols denote positive and negative potentials at the centers of the cells, for which the associated FACs are downward and upward, respectively. The large convection cells centered on the dawn and dusk flank sides are the usual solar wind-driven cells. The small near-midnight convection cell is related to the "unloading" process during the substorm EP [from *Kamide et al.*, 1994].

dominated by the MCS form and that the subsequent Hall conductance enhancement and westward electrojet (WEJ) intensification in the auroral region led to the development of a zonal current system which is equivalent to the traditional SCW configuration. *Lui and Kamide* [2003] proposed a non-MHD mechanism driving the MCS. For a small substorm event, *Liang et al.* [2004a, hereinafter referred to as LJ04] found that an enhancement of nightside convection and the appearance of a small postmidnight anticlockwise convection vortex immediately after the first pseudobreakup were signatures of the tail unloading process. During the subsequent evolution of this convection vortex and the associated auroral expansion, a transition from an initially MCS form to a zonal SCW configuration occurred.

[5] In this paper we continue to apply SuperDARN observations to the study of the morphology and dynamics of plasma convection in the postmidnight sector during the substorm EP. Four substorm events under different interplanetary magnetic field (IMF) conditions will be presented, with an emphasis on the formation and evolution of the postmidnight anticlockwise convection vortex (PoACV) and its relationship to the substorm EP process. In particular, both the timing of the PoACV formation with respect to the EP onset and the position of the PoACV relative to the auroral brightening region will be investigated. Possible mechanisms for the PoACV formation will be discussed. We also suggest an explanation of unsuccessful evolution of PoACV during IMF conditions dominated by negative By.

2. Equipment

[6] The main instruments for this study are the global SuperDARN HF radars in the Northern Hemisphere, the IMAGE (Imager for Magnetopause-to-Aurora Global Exploration) FUV (far ultraviolet) imager, and several magnetometer stations in the CANOPUS (Canadian Auroral Network for the OPEN Program Unified Study) and GIMA (Geophysical Institute of Magnetometer Array) chains.

[7] The SuperDARN radars [*Greenwald et al.*, 1995] use a multipulse transmission sequence to measure the autocorrelation function (ACF) of the echoes resulting from decameter-scale field-aligned irregularities in the ionospheric *E* and *F* regions. Each radar employs a single beam which is directed to 16 successive angular positions, with successive beams separated by 3.24°. The wedge-shaped field-of-view (FoV) is thus about 52° wide in for each radar, and the sequence of 16 beams is normally covered in a 2-min scan. The most important parameter obtained from the radar measurements is the Doppler velocity of the irregularities, which at *F* region heights yields a measure of the line-of-sight convective drift of the plasma. By combining the measurements from one or more pairs of radars with overlapping FoVs, a large-scale map of the two-dimensional convection velocity in a plane perpendicular to the geomagnetic field can be obtained every 2 min (or 1 min in the fast scan mode).

[8] Global auroral observations are taken by the IMAGE FUV imager. The FUV instrument employs three detectors, of which the Wideband Imaging Camera (WIC) data are used in this paper. The camera images the large-scale auroras in the Northern Hemisphere, in the spectral region 140–190 nm at an interval of ~2 min, roughly the same as the SuperDARN radar scan period. The FUV observations have been used to effectively identify substorm onset [*Frey et al.*, 2004]. In this paper, three of the four events analyzed were on the list of the event database of *Frey et al.* [2004]. The onset times determined from the FUV observations will be further verified by simultaneous ground-based magnetometer and geostationary satellite observations.

[9] The coordinates of magnetometer stations used in this paper are listed in Table 1. Satellite data from ACE and GOES are also employed in this research. In particular, the SWEPAM and MAG instruments on ACE are used to obtain upstream solar wind parameters, while the magnetometers on GOES-8 and GOES-10 yield the magnetic field observations at the geosynchronous-orbit plasma sheet. Figure 2 shows the global SuperDARN deployment and their FoVs (the Saskatoon-Kapuskasing and Prince George-Kodiak radar pairs are highlighted because these are the two main pairs are used in this paper for midnight and postmidnight sectors coverage) (Figure 2a), the locations of the CANOPUS and GIMA magnetometer sites (black dots), the easternmost site being the PBQ station of the Geological Survey of Canada (GSC) network (Figure 2b), and the ionospheric footprint of GOES-8 and GOES-10 (asterisks)

Table 1. Magnetometer Stations Used in This Paper

Station Name	Code	GG Lat, °N	GG Lon, °E	AACGM Lat, °N	AACGM Lon, °E
Arctic Village	Arctic	68.1	214.4	68.8	−96.7
Dawson	DAWS	64.1	220.9	66.0	−87.6
Eagle	Eagle	64.8	218.8	66.3	−90.0
Fort Churchill	FCHU	58.8	265.9	69.0	−27.7
Fort Simpson	FSIM	61.8	238.8	67.5	−67.4
Fort Smith	FSMI	60.0	248.0	67.7	−54.8
Fort Yukon	FtYukon	66.5	214.8	67.3	−95.0
Gillam	GILL	56.4	265.4	66.7	−28.1
Island Lake	ISLL	53.9	265.3	64.2	−27.8
Kaktovic	Kaktovic	70.1	216.4	71.1	−97.1
Pinawa	PINA	50.2	264.0	60.6	−29.3
Poste-de-la-Baleine	PBQ	55.3	282.3	65.7	−1.2
Rabbit Lake	RABB	58.2	256.3	67.3	−42.4

calculated from the Tsyganenko-89 model [*Tsyganenko*, 1989] with Kp = 3 (Figure 2c). The magnetic latitude (MLAT) contours shown on the background geographic map are based upon AACGM (Altitude Adjusted Corrected Geo-Magnetic) coordinate [*Baker and Wing*, 1989].

3. Data Analysis

[10] In the following we will present several substorm events. We shall focus on the evolution of ionospheric convection in the midnight and postmidnight sectors just before and after the substorm EP onset. For all the events we used the global map potential procedure [*Ruohoniemi and Baker*, 1998] to obtain the SuperDARN convection maps. However, we disabled the temporal median filtering to achieve better resolution of the rapid transitions of the convection patterns between consecutive scans.

3.1. Event of 22 February 2001

[11] The first interval considered is from 0830 to 0842 UT on 22 February 2001. The postmidnight sector is covered by the Saskatoon-Kapuskasing (S-K) radar pair. Magnetometer data from several CANOPUS stations in the vicinity of the S-K FoV are given in Figure 3. This was a moderate substorm with a maximum magnetic disturbance of ∼−400 nT. The top panel gives the magnetic elevation angle derived from the GOES-10 magnetic field observations. The GOES-10 magnetic fields have been converted to the local VDH coordinate system, in which H is antiparallel to the dipole axis, V lies in the meridian plane and is positive outward, and D completes the right-hand orthogonal system and is positive eastward. The magnetic elevation angle θ_B is defined as

$$\theta_B = \arctan(-B_H/B_V). \quad (1)$$

In the bottom panel of Figure 3 we also give the Pi2 oscillations at PINA station resulting from passing the magnetic H-component through a bandpass filter for periods from 40 to 150 s. The auroral breakup observed by the IMAGE FUV camera was at 0833:07 UT. This onset time is supported by Figure 3, which shows that the magnetic dipolarization seen at GOES-10, the sharp negative

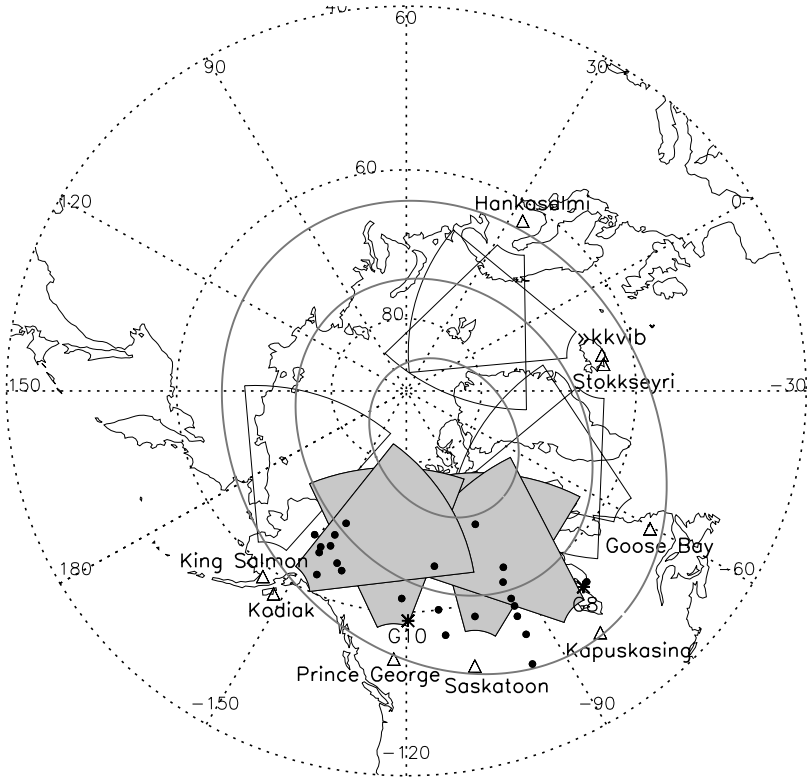

Figure 2. Locations of SuperDARN radars in the Northern Hemisphere and their FoVS, CANOPUS and GIMA magnetometer stations (black dots), and the ionospheric footprints of the GOES-8 and GOES-10 satellites (asterisks). AACGM latitudes 60° to 80° at 10° intervals are shown using lighter curves.

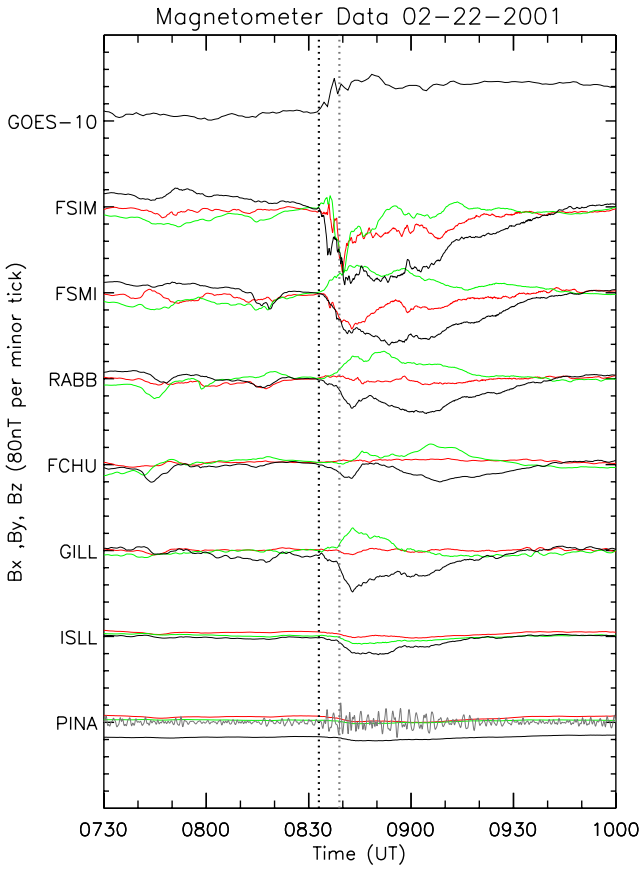

Figure 3. Top panel gives the magnetic elevation angle determined from GOES-10 observation on 22 February 2001. The other panels show the magnetometer data from a few CANOPUS stations. Black, red and blue lines denote the H, D, and Z components of the magnetic field. The scale is 4°, 80 nT, and 0.8 nT per tick for magnetic elevation angle, magnetic fields, and Pi2 pulsations, respectively. The first vertical dotted line indicates the substorm EP onset time identified from IMAGE FUV observation, and the second lighter dotted line indicates the time of the PoACV formation.

magnetic deviations at FSIM and FSMI, and the Pi2s at PINA all began roughly at about 0833 UT.

[12] The solar wind observations taken by the ACE satellite are shown in Figure 4. From top to bottom, the four panels are the three components of IMF and the northern polar cap (PCN) magnetic activity index. The PCN index is obtained from the near-pole magnetometer stations at Thule in Greenland (85.4° MLAT) [*Troshichev et al.*, 1988]. It was found that there is usually a high correlation between the polar cap magnetic index and the solar wind electric field [*Kan and Lee*, 1979]. The propagation time of the solar wind from ACE to the subsolar magnetopause, together with the response time of polar ionosphere, was estimated by evaluating the cross-correlation analysis between the PCN index and the solar wind electric field, which peaked at a lag of ~82 min in this event with a correlation coefficient of 0.83, so the ACE data were shifted according to this estimated delay. The IMF was dominantly southward before 0850 UT, though there were several short-lived positive Bz excursions. The IMF By component was dominantly positive after ~0740 UT. About 10 min before the onset time at ~0833 UT there were two consecutive short northward IMF excursions, leading to a reduction of solar wind-magnetosphere coupling which was indicated by a decrease of the PCN index. This reduction of the solar wind-magnetosphere coupling might have acted as the external trigger of the substorm EP onset [*Lyons et al.*, 2003]. However, determination of the substorm trigger mechanism is not the purpose of this paper.

[13] A series of the ionospheric plasma convection maps based on SuperDARN radar measurements taken from 0830 UT to 0842 UT are presented in Figure 5. From 0830 to 0832 UT, an interval which marked the end of the substorm growth phase, the large-scale convection pattern in the postmidnight-morning sector was a single convection cell centered at ~4.2 MLT. In the postmidnight sector from 0 to 3 MLT, the flows were dominantly equatorward. At lower latitudes (≤70° MLAT) the flows was in general southeastward and rather weak in magnitude. The postmidnight convection pattern changed substantially from 0832 to 0834 UT, during which time the substorm auroral breakup region was seen in the evening sector around 20.5–22 MLT. Note that the postmidnight flows at this stage started to show evidence of zonal shear; the flows were dominantly westward above 72° MLAT but almost purely eastward at

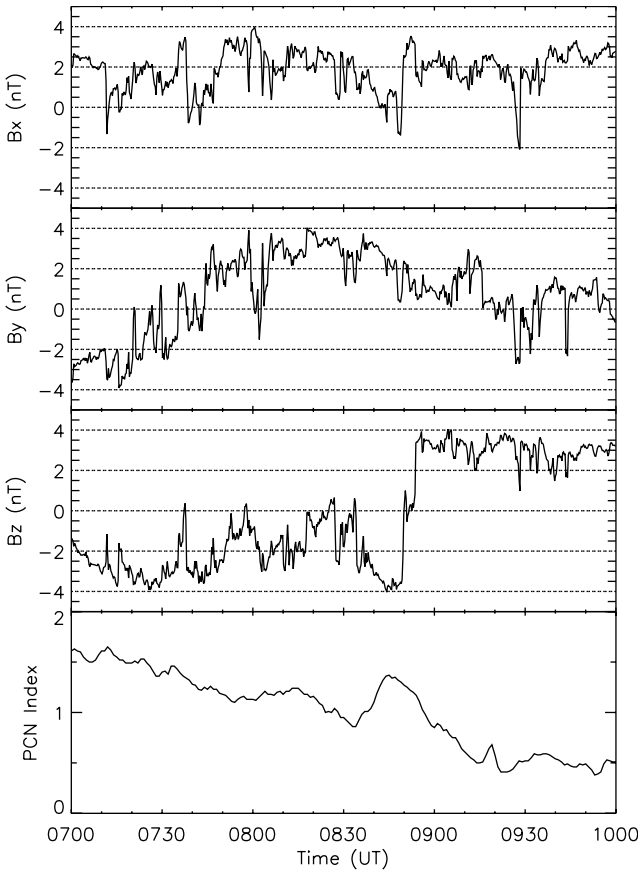

Figure 4. IMF observations from ACE satellite (shifted by 82 minutes) on 22 February 2001. The IMF components are in GSM coordinates. The bottom panel shows the PCN index.

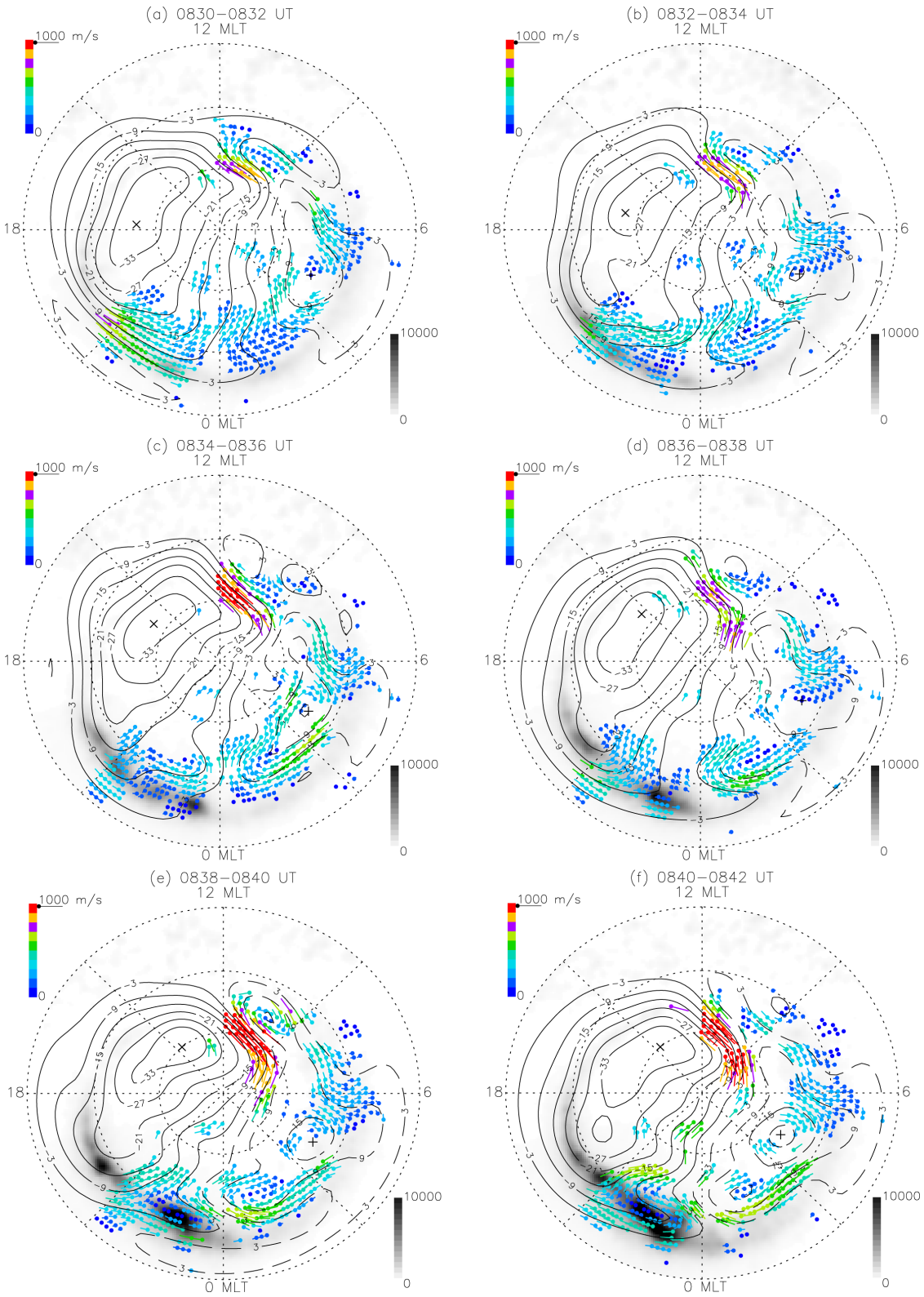

Figure 5. Six frames of global SuperDARN convection and IMAGE FUV images from 0830–0842 UT on 22 February 2001. The dotted latitude circles represent 60°, 70°, and 80° MLAT. The color scale for the convection velocity and the grayscale for the NASI emission intensity are shown at the upper left and lower right corners of each frame, respectively.

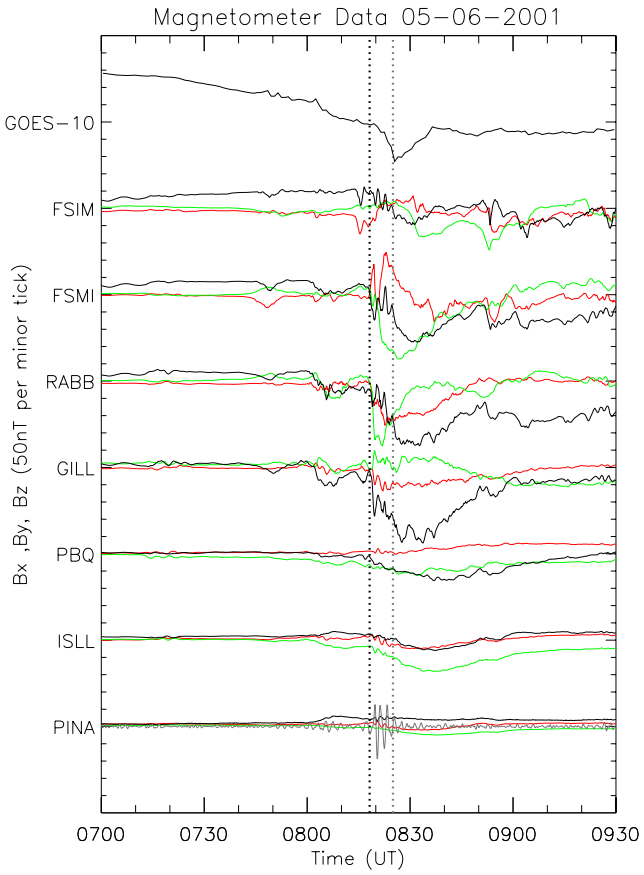

Figure 6. Magnetic elevation angle determined from GOES-10 observations and magnetometer data from a few CANOPUS stations on 6 May 2001. The format is the same as in Figure 3, except that the scale here is 4°, 50 nT, and 4 nT per tick for magnetic elevation angle, magnetic fields, and Pi2 pulsations, respectively. The first vertical dotted line indicates the substorm EP onset time identified from IMAGE FUV observation, and the second lighter dotted line indicates the time of the PoACV formation.

lower latitude. The zonal flow shear continued to develop after the onset, and the eastward auroral flows at about 70° MLAT were considerably enhanced as seen from the next two frames from 0834 to 0838 UT. Finally, at 0838–0840 UT, about 6 min after the onset, a well-defined anticlockwise convection vortex formed. It is centered at 1.2 MLT and 72.5° MLAT in the postmidnight sector, while the preexisting dawn cell is still visible in the early morning sector. At the same time, in the vicinity of the region of brightest auroral emissions at ~22.5 MLT, the flows were diverted around the zone of intensified aurora, eastward at higher latitudes and westward at lower latitudes, forming an intruding part of the original dusk cell. Inside the intensified aurora the convective flow was suppressed, in accordance with *Yeoman et al.* [2000] and *Khan et al.* [2001]. This intruding flow reversal region was found to extend into the postmidnight sector. Despite the small number of data points at lower auroral latitudes, there is still evidence that an east-to-west flow reversal at least at about 67° MLAT and 1.2 MLT. Unlike the evening sector, the flow reversal region in the postmidnight sector did not correspond to intense auroral intensification, probably because conditions were unfavorable for the onset of the magnetospheric-ionospheric feedback instability which would have led to auroral brightening [*Atkinson*, 1970]. It is important to notice that the intruding flow reversal region shown in Figure 5e could be equivalently viewed as the lower "unloading cell" in KY94 model (see Figure 1) that is attached to a "background" dusk cell seen in previous frames. Thus the overall convection pattern in Figure 5e is consistent with the two unloading cells postulated by KY94. Those convection features persisted during the interval 0840–0842 UT. In this event the focus of the PoACV was 2–3° higher in latitude than and 2.5–3 hours MLT to the east of the brightest auroral region around 22.5 MLT (There was also bright aurora around 20 MLT in the dusk sector). Unfortunately, after 0844 UT the number of radar echoes in the postmidnight sector declined, probably due to the strong absorption in *E* and *D* regions or to unfavorable propagation conditions resulting from the enhanced *E* region electron densities. As a result, further investigation of the subsequent motion and evolution of this PoACV was not possible.

3.2. Event of 6 May 2001

[14] Figure 6 shows the magnetometer observations from several CANOPUS stations and the PBQ station from 0700 to 0930 UT on 6 May 2000. The top panel shows the variations of the magnetic field elevation angle defined by equation (1) from the GOES-10 observations. The auroral breakup determined from the IMAGE FUV observations was at 0819:42 UT. A negative magnetic bay first appeared at PBQ and GILL stations at 0818:30 UT, and the Pi2 bursts at PINA shown in the bottom panel began roughly at the same time. However, the magnetic field elevation angle observed by GOES-10, which was then at ~23 MLT, decreased sharply after 0819 UT and subsequently increased at 0826 UT. The FUV images (seen in Figure 8 later) reveal that the initial onset region was at midnight, to the east of GOES-10. The subsequent expansion of the SCW would likely have led to stretching of the field line at GOES-10, due to the upward field-aligned current (FAC) near the western edge of the SCW. As soon as the SCW expansion had passed the GOES-10, the dipolarization occurred, which would explain the bipolar feature in the GOES-10 observations.

[15] The IMF parameters observed by the ACE satellite are shown in Figure 7. A shift of ~85 min was made to the ACE data to achieve the best correlation coefficient (0.72) between the solar wind electric field and the PCN index. The IMF Bz component was dominantly negative before 0850 UT but for several short intervals almost reached zero. The IMF By component was positive before ~0900 UT and in general was larger in magnitude than Bz.

[16] Figure 8 gives a series of global convection maps for this event. Similar to Figure 5a in the previous event, Figure 8a shows that at 0816–0818 UT, the end of growth phase, the dawnside convection was a large single cell. The flows at 70° MLAT were dominantly equatorward in the midnight and postmidnight sectors. At 0818–0820 UT, when the substorm auroral breakup began around magnetic midnight, those strong equatorward flows in the postmidnight sector diminished. Later at 0820–0822 UT, the postmidnight convection pattern at ~3 MLT developed

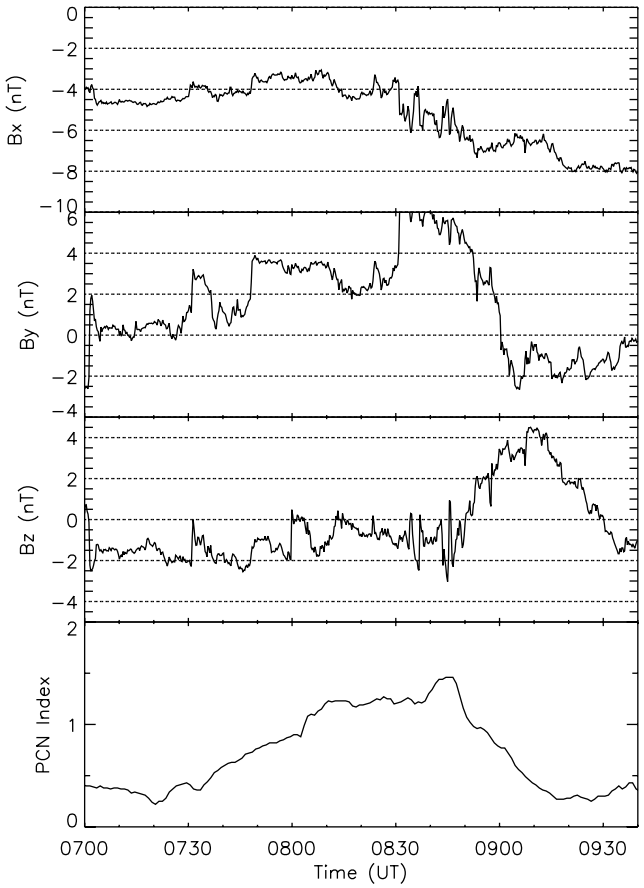

Figure 7. IMF observations from the ACE satellite (shifted by 85 min) and the PCN index on 6 May 2001.

more zonal shear below and above 70° MLAT, similar to that seen in Figure 5b. The zonal shear at ~3 MLT continued to develop in the interval 0822–0824 UT, and the flows below 70° MLAT became increasingly eastward. At the same time, a very strong enhancement of westward flows occurred at ~67° MLAT in the evening sector, which is likely the signature of the "auroral westward flow channel" [*Parkinson et al.*, 2003] and/or the subauroral polarization stream (SAPS) [*Foster and Vo*, 2002; A. V. Koustov et al., Observations of high-velocity SAPS-like flows with the King Salmon SuperDARN radar, submitted to *Annales Geophysicae*, 2006, hereinafter referred to as Koustov et al., submitted manuscript, 2006]. Though again there were relatively few data points at subauroral latitudes in the postmidnight sector, an east-to west flow reversal region was still visible up to ~1.4 MLT and 67–68° MLAT, wrapping around the bright aurora. At 0824–0826 UT a small PoACV structure began to form with focus at ~2.7 MLT, and it became well established by the next radar scan interval 0826–0828 UT. As in the previous event, that vortex was located near the west end of the broader morning cell component of the two-cell convection pattern. In this event we found that the PoACV was slightly higher in latitude than the auroral intensification region, but again ~2.5 MLT to the east. The PoACV gradually migrated toward the dawn meridian with the vortex focus moving eastward in the next few frames from 0828 to 0836 UT. By 0834–0836 UT, the anticlockwise vortex had expanded to be the dominant feature cell of the morning convection pattern.

3.3. Event of 2 February 2002

[17] In the previous two cases, there were some IMF variations around the substorm onset time. The question arises as to whether the dynamic changes of postmidnight convection were directly driven by the solar wind or driven through the unloading of stored magnetotail energy associated with substorm process. We now will present a substorm event during fairly stable IMF conditions. The magnetometer data and the magnetic field elevation angles measured by GOES-8, in the same format as those in Figures 3 and 6, are shown in Figure 9. Unfortunately, there was neither IMAGE FUV data nor observations from the NORSTAR all-sky-imager during the event interval. The meridian scanning photometer (MSP) observations at GILL and PINA are shown in the top two panels. An abrupt poleward expansion of intensified auroras was first seen from PINA MSP at 0555 UT, and the dipolarization onset observed at GOES-10 began at the same time. The negative magnetic bay at GILL and the Pi2 pulsations at PINA began slightly later at ~0556 UT. From these observations we can infer that the substorm EP onset probably occurred during the 0554–0556 UT radar scan. This was an intense but short-lived event. The dipolarization observed by GOES-8, the auroral observations from the GILL MSP, and the negative magnetic bays seen at GILL and PBQ all indicated that this substorm disturbance lasted no more than 15 min.

[18] Figure 10 shows both the IMF measurements from ACE and the PCN index. The IMF Bz was constantly negative, with very large and stable magnitude (−10 to −12 nT). The IMF By oscillated between +4 and −2 nT. However, considering the dominant negative Bz values, the IMF By variations should not have affected the solar wind-magnetospheric coupling significantly. There was no apparent external IMF trigger for this substorm. Since both the IMF and PCN indices were rather stable, the cross-correlation analysis does not apply here. We can, however, estimate the time delay from ACE to the ionosphere based upon the X-distance of the ACE and the observed solar wind velocity (~330 km/s). The propagation delay of the solar wind from ACE to the bow shock and then to the subsolar magnetopause is about 74 min, and we add 10 min to account for the global high-latitude ionospheric response to the magnetopause reconnection. The above estimate is somewhat arbitrary but the ambiguity will not affect greatly our research goals, due to the stable IMF condition during this event.

[19] The evolution of the convection pattern during this substorm is shown in Figure 11. At 0552–0554 UT, the convection pattern still had showed typical growth phase features, namely an active morning cell centered at the dawnside flank and strong equatorward flows in the midnight sector. However, from 0554 to 0556 UT (the estimated onset time interval) the original strong equatorward flows across ~70° MLAT in the midnight sector decayed, and a clear small anticlockwise vortex with focus at 0.7 MLT formed in the postmidnight sector. In contrast to the previous two events in which the final formation of the PoACV vortex lagged the onset by 6–8 min, in this event the onset and vortex formation seemed to be concurrent

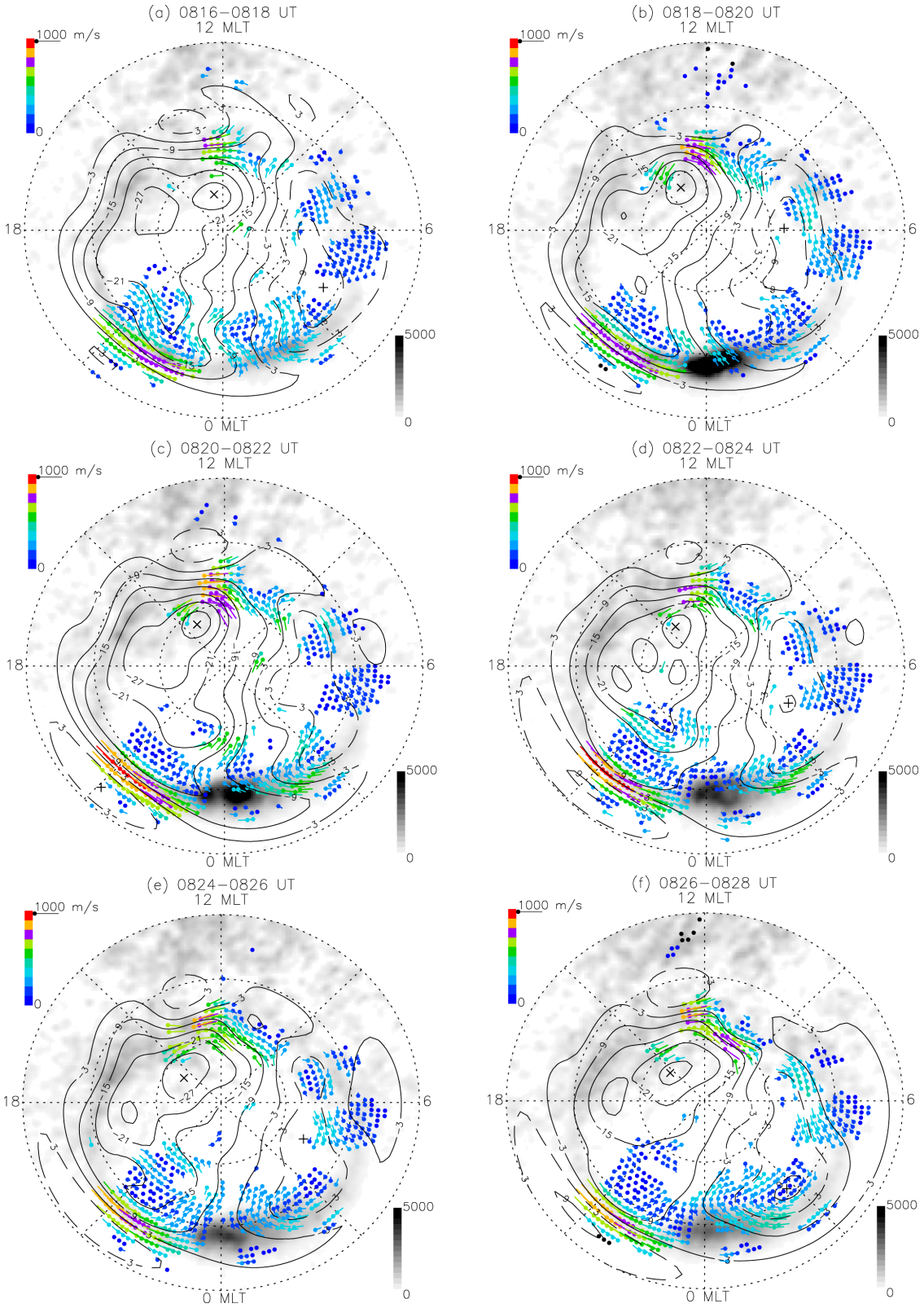

Figure 8. Ten frames of global SuperDARN convection and IMAGE FUV images from 0816 to 0836 UT on 6 May 2001. The format of each frame is the same as in Figure 5.

within the 2-min radar resolution. However, we must keep in mind that due to the absence of global auroral observations, the onset timing is somewhat ambiguous. It is possible that the EP onset actually began a couple of minutes earlier, in the region void of observations. In fact, a careful inspection of Figure 11a gives a hint that a small anticlockwise vortex was already began to form at 0552–0554 UT. This vortex grew in intensity and size at 0556–

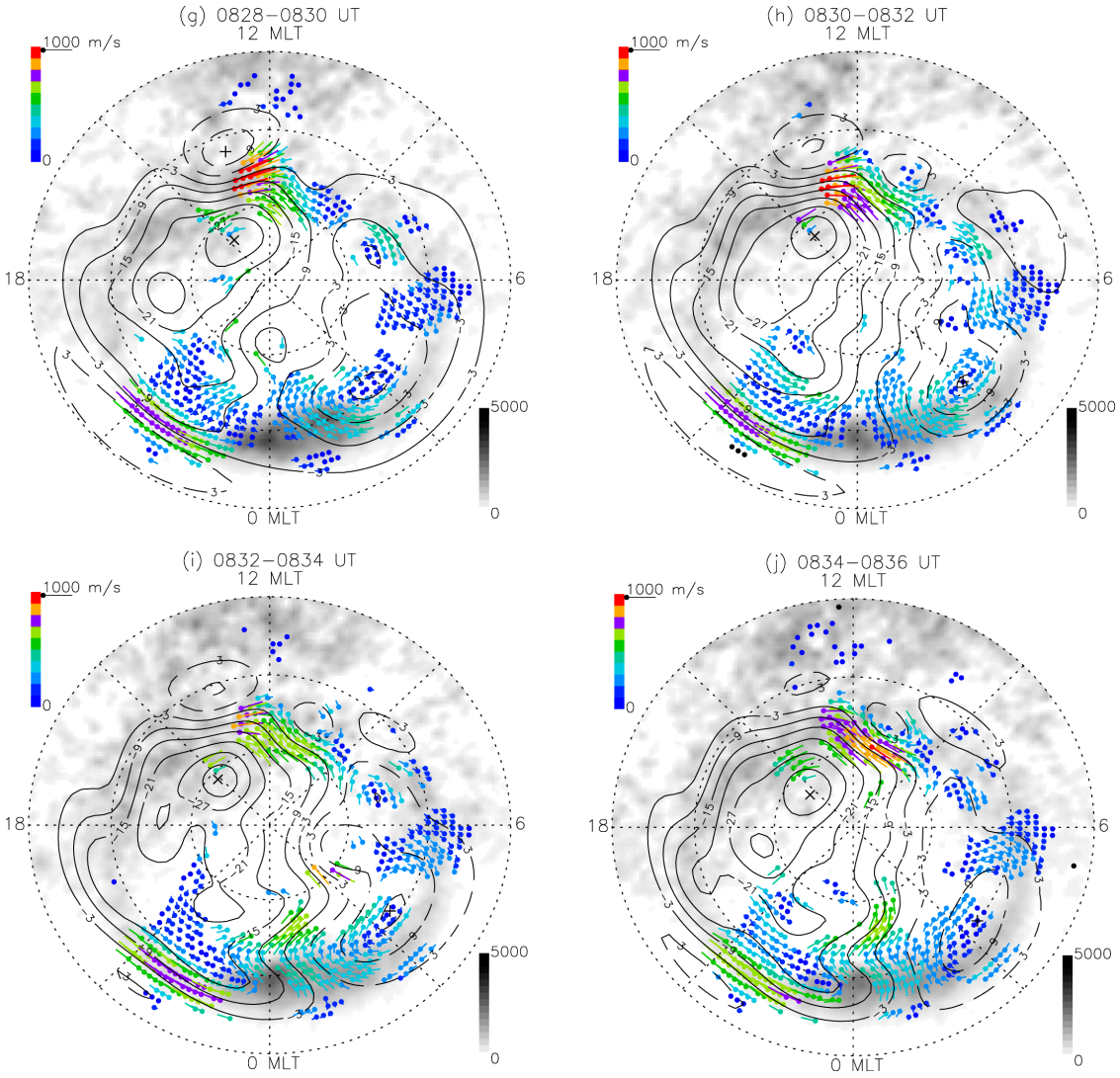

Figure 8. (continued)

0558 UT and had its eastern boundary adjacent to the postmidnight portion of the preexisting dawn cell. At 0600–0602 UT, the originally small PoACV had combined with the postmidnight portion of the preexisting dawn cell and formed a larger anticlockwise cell. The cell continued to grow in magnitude and size during the 0602–0604 UT scan. By 0606–0608 UT, this cell had become the dominant feature of the larger morning cell in the postmidnight-predawn sector.

3.4. Event of 17 February 2002

[20] In this event the substorm activity was observed by the GIMA magnetometer chains and a few western stations of CANOPUS. The postmidnight sector was covered by Prince George-Kodiak radar pair. The magnetometer data from some GIMA and CANOPUS stations, and also the magnetic field elevation angles measured by GOES-10, are given in Figure 12. This was a fairly weak event in terms of magnetic and auroral activity. The auroral breakup frame from IMAGE FUV observations is at 1139:21 UT, while the negative magnetic bays at the DAWS and Eagle stations, as well as the Pi2 pulsations at FSIM began at ~1139 UT. The magnetic elevation angles observed at GOES-10 show a decreasing trend until ~1150 UT, but in an oscillatory pattern. After 1150 UT, the magnetic elevation angle rose very slowly, implying a rather small dipolarization effect. We interpret this lag as a propagation effect, namely, an eastward expansion of the substorm from the Eagle and DAWS stations to the position of GOES-10. Considering the fact that this substorm event was fairly weak and that GOES-10 was at ~3 MLT around the onset time, it is not surprising that only a weak dipolarization was seen there.

[21] Figure 13 shows the IMF observations for this event at the ACE satellite. A shift of ~70 min was made to the ACE data to achieve the best correlation coefficient (0.70) between the solar wind electric field and the PCN index. Near the onset at 1139 UT the IMF Bz component had some variations between 2 and −2 nT but the IMF By was strongly negative and had a magnitude much larger than Bz. It is well known that such a By-dominated IMF orientation may result in dawn-dusk asymmetry of the high-latitude ionospheric convection pattern [e.g., *Reiff and Burch*, 1985; *Cowley and Lockwood*, 1992].

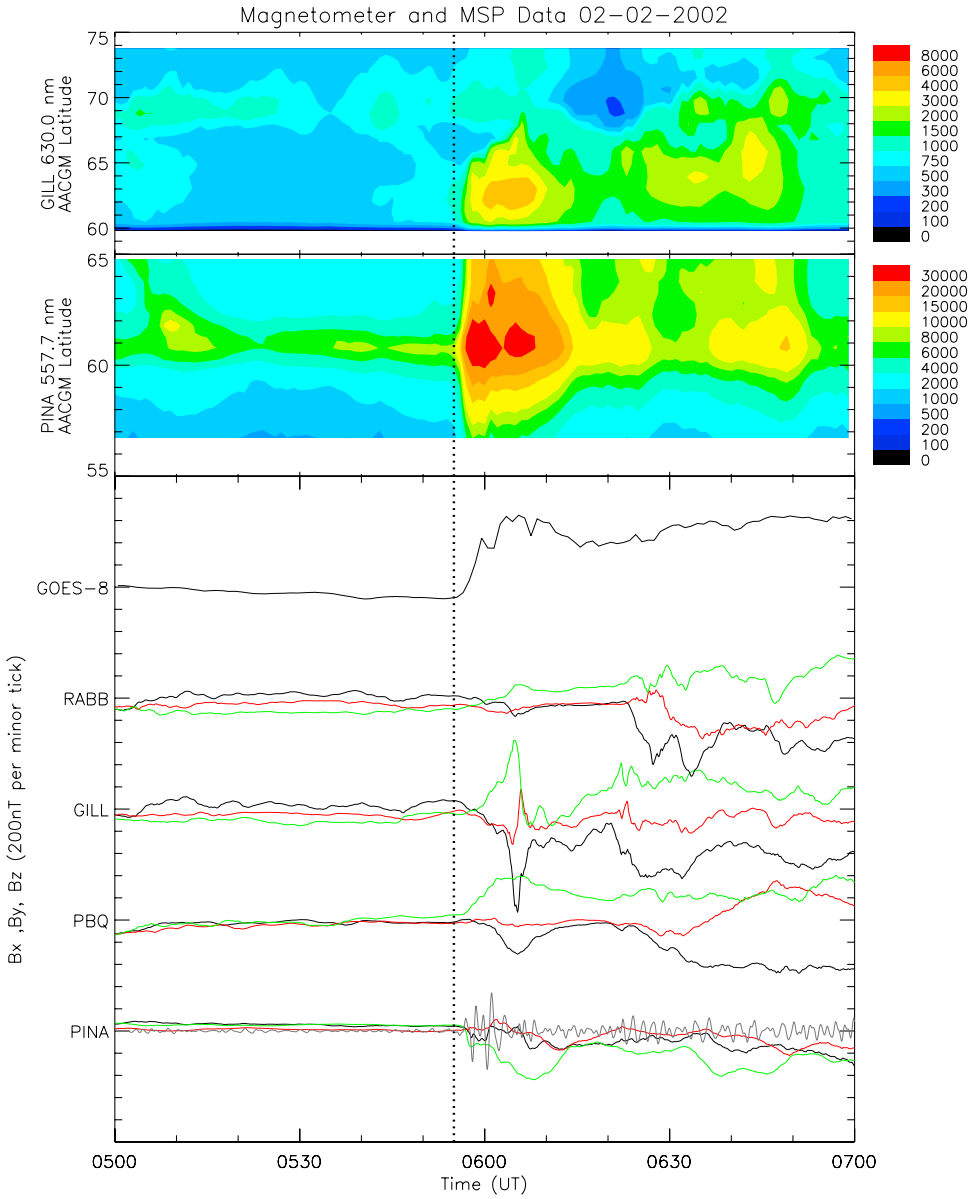

Figure 9. The top two panels show the MSP observations at GILL for the red line (630.0 nm) and at PINA for the green line (557.7 nm) on 2 February 2002. The other panel has the same format as in Figure 3 and 6, except that the scale here is 10°, 200 nT, and 20 nT per tick for magnetic elevation angle, magnetic fields, and Pi2 pulsations, respectively. A vertical dotted line indicates the substorm EP onset time estimated from the available observations. In this event the formation of the PoACV was roughly concurrent with the substorm onset.

[22] Figure 14 gives a series of convection maps for this event. At 1136–1138 UT, just prior to the substorm onset, the flows at latitudes less than 71° MLAT in the postmidnight sector were dominantly equatorward and rather weak. Soon after the substorm onset at 1139 UT, there was again a clear increase in the eastward convection flows at lower latitudes in the postmidnight sectors. The eastward convection continued to increase from 1138 to 1156 UT. On the other hand, though the premidnight convection measurement was totally absent for this event, Figures 14d and 14e still show an east-to-west flow reversal region at 65–67° MLAT in the postmidnight sector, wrapping around the intensified auroras. However, the difference between this and all previous events is that, up to 1156 UT, 15 min after the substorm onset, the eastward convection continued to increase until it reached its maximum event value (∼1 km/s) at ∼ 69° MLAT, but there was no indication of the formation of a PoACV. There was an anticlockwise cell with focus at ∼80° MLAT, 2.5 MLT from 1150 UT, but this cell was located at quite high latitudes and extended well into the dayside and thus was not likely to have been directly associated with the substorm process. We will discuss the nature of this high-latitude cell in the following section. At 1156–1158 UT there were some a hint of an anticlockwise vortex forming at 2–4 MLT, ∼72.5 MLAT. This could have been the initial signature of a PoACV, but

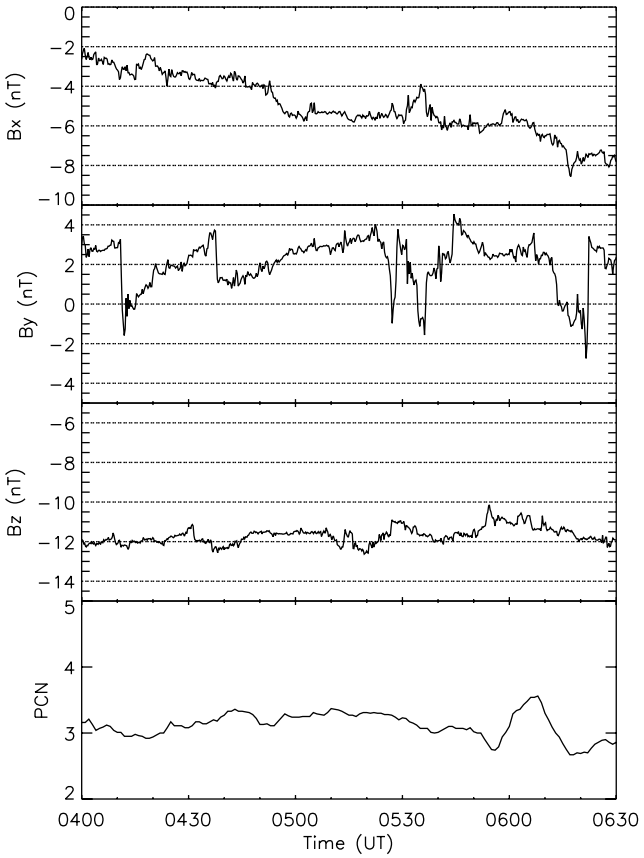

Figure 10. IMF observations from ACE satellite (shifted by 84 minutes) and the PCN index on 2 February 2002.

this vortex quickly dissipated in the next 2–4 min and showed no subsequent evolution. In summary, we interpret this event as an unsuccessful PoACV evolution.

4. Discussion

[23] Together with the event reported by LJ04, we have found a few substorm events of different disturbance levels and subject to various IMF orientations, but all illustrate similar postmidnight convection patterns after the substorm EP onset. We believe those changes are closely associated with the substorm dynamics. The radar observations presented in this paper show the presence of the PoACV during the substorm EP and thus they provide support for the KY94 model. In all events, shortly after the substorm onset, flows at auroral latitudes became increasingly eastward, and an anticlockwise vortex developed in the postmidnight sector (except for event D, which we will discuss later). In events A and B, for which global auroral images are available, we found that the PoACV was clearly established within 6–8 min of the substorm EP onset. More importantly, as seen from Figure 3, in event A the magnetic H-component at RABB and ''Manitoba-line'' stations (ISLL-GILL-FCHU) first showed a slow decrease after the onset but then dropped more sharply after the formation of the PoACV. Also, for event B, Figure 6 shows that the H-components at the RABB, FSMI, and FSIM stations showed some oscillations after 0819 UT but a definite ''magnetic bay'' occurred only after the emergence of the PoACV. Thus we infer that the formation of the PoACV also marked the complete establishment of the WEJ and the associated substorm current system over a wide MLT range on the nightside. On the other hand, the PoACV was ~3° higher in latitude than the brightest auroral region in event A but only slightly higher in event B. In both events the foci of the anticlockwise vortices were located 2.5–3 hours MLT east of the brightest auroral region. The anticlockwise cell (upward vorticity) implies downward FACs [*Sofko et al.*, 1995], while the bright optical aurora is usually associated with the precipitating electrons and thus upward FACs. The inferred substorm closure current system in events A and B showed a northeast-to-southwest alignment and therefore can be resolved into a meridional component and a zonal component, with the latter corresponding to the traditional SCW configuration. In the above events, particularly for event B, the zonal SCW geometry is more pronounced.

[24] Event C is somewhat different in that the formation of the PoACV at 0554–0556 UT occurs almost simultaneously with, or at least quickly follows the substorm EP onset (as mentioned before, there was some ambiguity in the onset timing for this event). In this event the auroral observations come only from the one-dimensional measurements of the MSPs at GILL and PINA (both at ~23.5 MLT), so the exact location of the auroral breakup region is not known. However, there are several clues to the location of the breakup region. First, the negative magnetic bay at PBQ (~0.8 MLT) began slightly later, and was much weaker in magnitude, than that at GILL, implying that the onset region is closer to the latter. Second, because there was very little magnetic perturbation at RABB (~22.5 MLT) until ~0603 UT, the onset region must have been well to the east of RABB. Also, in Figure 11b (the scan at the onset time) we notice that in comparison with the previous frame, the flows between 22.5 to 0.5 MLT below 68° MLAT are strongly suppressed. We assume that the flow suppression region was associated with a suddenly intensified region of aurora, as proposed by *Yeoman et al.* [2000] and *Khan et al.* [2001], and as we have identified in event A (Figure 5e). Considering all the above clues, we deduce that in this event the auroral breakup associated with the EP onset was located southwest of, but much closer in longitude to, the PoACV than in previous two events. The inferred substorm current system thus has more of a meridional than zonal configuration. For the small substorm event under dominantly IMF Bz+ conditions in LJ04, it was also found that a PoACV emerged almost simultaneously with the auroral breakup, and that the focus of the vortex was ~3° MLAT higher in latitude than but only ~0.5 hours MLT east of the brightening arc. It is not unreasonable to suggest that the relative longitudinal separation between the PoACV and the auroral brightening region was the major factor determining the lag between the PoACV formation and the substorm EP onset. When the PoACV and the initial auroral breakup happen to occur within a small longitudinal separation, the PoACV emerges quickly after the onset; for a greater separation, there can be a time delay of a few minutes before the PoACV formation.

[25] In events A, B and D, we have seen another consistent feature of the nightside convection pattern,

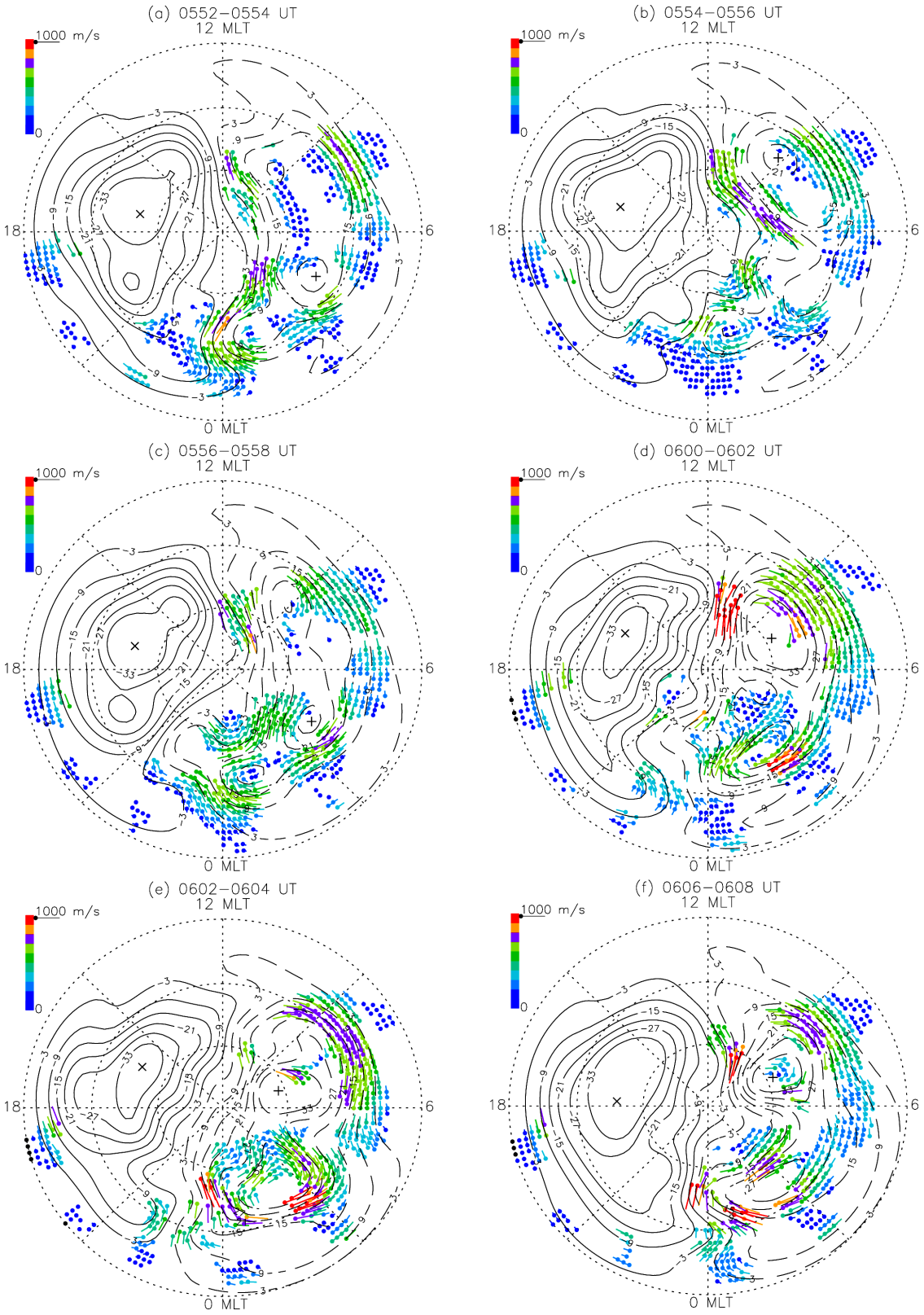

Figure 11. Six frames of global SuperDARN convection from 0552 to 0608 UT on 2 February 2002. The format of each frame is the same as in Figure 5.

namely, an east-to west flow reversal region at lower latitudes (~67° MLAT), wrapping around the bright auroras. In event C, however, since the equatorward border of the bright aurora is at very low latitude (<60° MLAT) as seen from PINA MSP observations, the westward flows, which are expected to be at latitudes close to or even lower than the auroral equatorward border, could not be observed by our radar. Nevertheless, hints of a developing east-to-

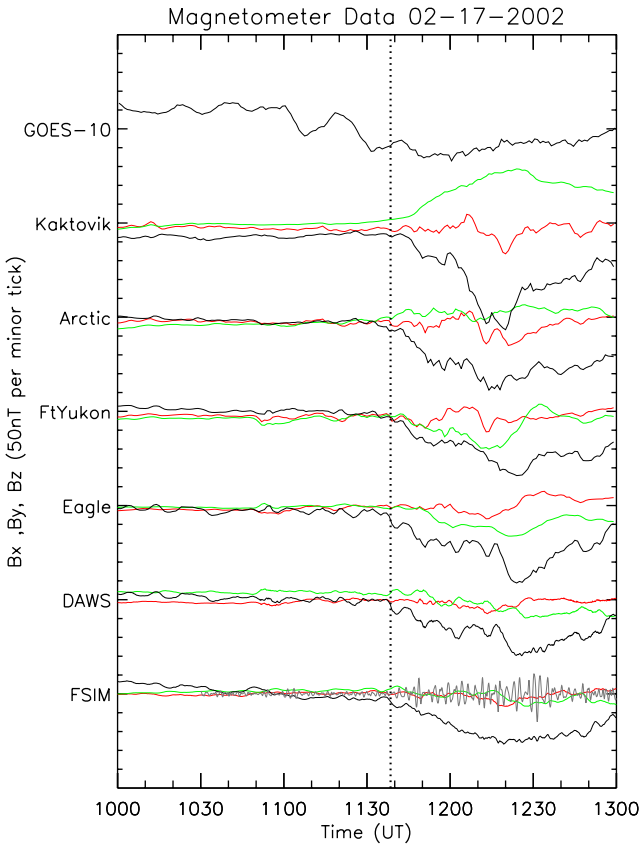

Figure 12. Magnetic elevation angle determined from GOES-10 observations and magnetometer data from a few CANOPUS and GIMA stations on 17 February 2002. The format is the same as in Figure 3, except that the scale here is 2°, 50 nT, and 4 nT per tick for magnetic elevation angle, magnetic fields, and Pi2 pulsations, respectively. A vertical dotted line indicates the substorm EP onset time identified from IMAGE FUV observation. There was no well-established PoACV in this event.

west flow reversal region around the midnight sector can still be identified in Figure 11a, the frame just before the substorm onset. Such an east-to-west flow reversal in the premidnight sector is an intruding part of the dusk cell and is sometimes associated with the Harang discontinuity geometry [*Koskinen and Pulkkinen*, 1995; *Bristow et al.*, 2001]. It also represents a transition from the WEJ (eastward flows) in the auroral region to the SAPS-like westward flows near and/or south of the equatorward border of the auroral oval [*Parkinson et al.*, 2003; *Foster and Vo*, 2002; Koustov et al., submitted manuscript, 2006]. This flow reversal region progressively expands into the postmidnight sector during the substorm EP, which is consistent with the observations that SAPS may extend well into the postmidnight sector during strongly magnetically disturbed periods [*Huang et al.*, 2001; *Foster and Vo*, 2002]. Using both high-time resolution radar and magnetometer observations, *Wild and Yeoman* [2000] studied the azimuthally propagating vortical currents (APVCs) associated with upward FACs during substorms. Those APVC structures were found to propagate eastward in the postmidnight sector away from the onset region, which is compatible with the scenario of postmidnight intrusion of the east-to-west flow reversal (upward FAC) region. One of the consequences of this postmidnight intrusion of the flow reversal region is that it becomes closer in longitude to the PoACV located at higher latitude. For example, in Figure 5e of event A, the east-to-west flow reversal region was visible up to 1.2 MLT, which is roughly the same longitude as the focus of the PoACV. Although the most intense upward FACs in this event are undoubtedly located in the brightest auroral region in the evening sector well to the west of the PoACV, a smaller portion of upward FACs also occurred in the flow reversal region at ~67° MLAT in the postmidnight sector. This portion would form a primarily MCS geometry with the PoACV at higher latitude. This result again reveals the coexistence of the meridional and zonal components of the substorm current system.

[26] In a recent theoretic study, J. R. Kan et al. (Substorm expansion onset and ring current injection conjecture, manuscript in preparation for *Annales Geophysicae*, 2006) also suggested that a realistic substorm current system would consist of both the meridonal and zonal current systems. The ionospheric closure of the meridional current loop is dominantly the Pedersen current associated with equatorward electric fields, of which the generation mechanism will be discussed later. The zonal current loop is closed in the ionosphere via a westward current, i.e., the WEJ, which is a combination of both the Pedersen current and Hall current, associated with both convective electric fields arising from magnetospheric sources and polarization

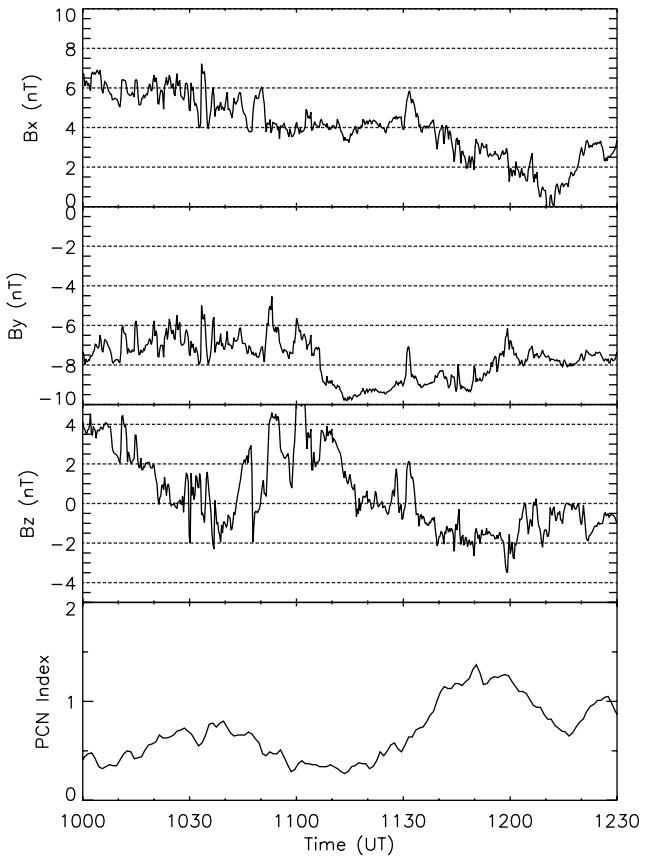

Figure 13. IMF observations from ACE satellite (shifted by 70 min) and the PCN index on 17 February 2002.

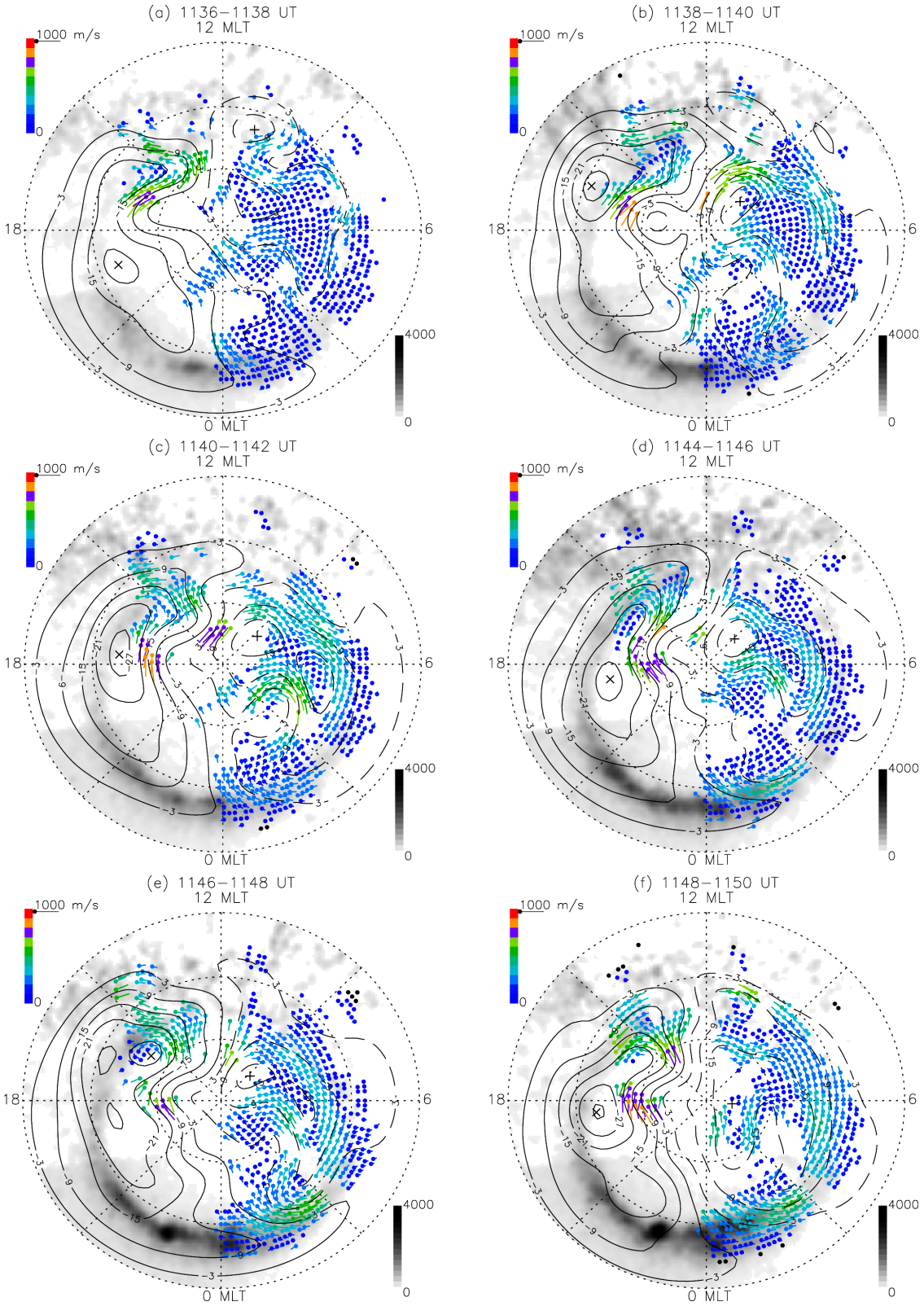

Figure 14. Ten frames of global SuperDARN convection and IMAGE FUV images from 1138–1200 UT on 17 February 2002. The format of each frame is the same as in Figure 5.

electric fields developed within a high-conductance auroral slab (sometimes referred to as a "Cowling channel") in the ionosphere. The substorm current system geometry is inherently related to the distribution and the relative importance of the ionospheric Hall and Pedersen conductances. During a substorm EP, there would be a positive feedback between the FACs and ionospheric conductances in specific regions, usually where strong auroral intensifications occur,

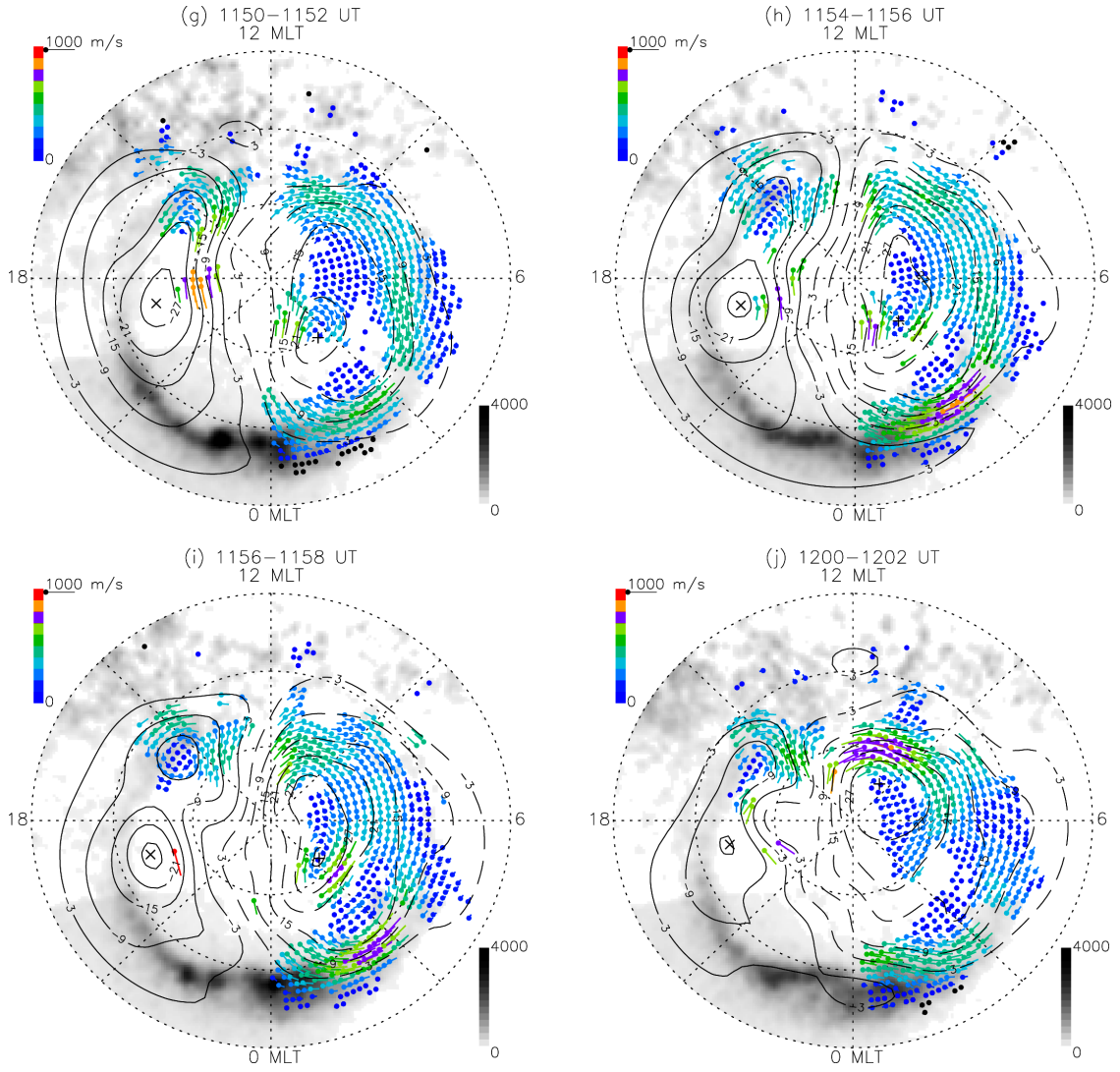

Figure 14. (continued)

leading to a significant change of the local Hall and Pedersen conductances as well as the ratio between them. Such an interaction process is highly dynamic and contingent upon many magnetospheric and ionospheric parameters, with the result that the actual substorm current system configuration differs from case to case.

[27] Now we discuss the possible generation mechanisms for the PoACV during the substorm EP. One scenario is that this vortex is part of the twin-vortex convection system generated by nightside reconnection [*Cowley and Lockwood*, 1992]. The foci of the twin-vortex flows are located at each end of the nightside merging gap. An illustrative diagram of this model is given in Figure 15a. Nightside tail reconnection and near-geosynchronous onset have long been two basic components of the substorm scenario, though their relative timing and cause-effect relationship remains controversial [e.g., *Lui*, 2001]. A new perspective of their physical relationship was proposed on the basis of experimental results by *Liang et al.* [2004b] and was later given a theoretical basis in the work of *Voronkov* [2005]. *Provan et al.* [2004] showed that after the substorm EP onset, the dawn-to-dusk polar cap potential usually increases significantly, which provides evidence of nightside reconnection. In this paper we will not use the cross-polar cap potential drop estimated form SuperDARN convection as a measure of reconnection process, because in all of our events there was a scarcity of data in the dusk sector, which may cast doubt on the validity of cross-polar cap potential estimates. *Grocott et al.* [2002] performed an event study to demonstrate the excitation of twin-vortex flow in the nightside ionosphere during a substorm EP; the focus of the postmidnight vortex was at $\sim$73° MLAT and $\sim$1 MLT, which is quite comparable to our results.

[28] However, there is one piece of observational evidence in our events that is not easily explained by the above nightside reconnection-driven mechanism. In events A and B, the formation of the PoACV was preceded by a strong enhancement of eastward convection at latitudes $\leq$70° MLAT. On the other hand, there was no obvious enhancement of the flow intensity at higher latitudes in the same time sector. For example, as can be seen from Figure 5e, the lower part of the PoACV was marked by flows that were significantly greater in magnitude than in the preonset frame (Figure 5a), while the upper part of the

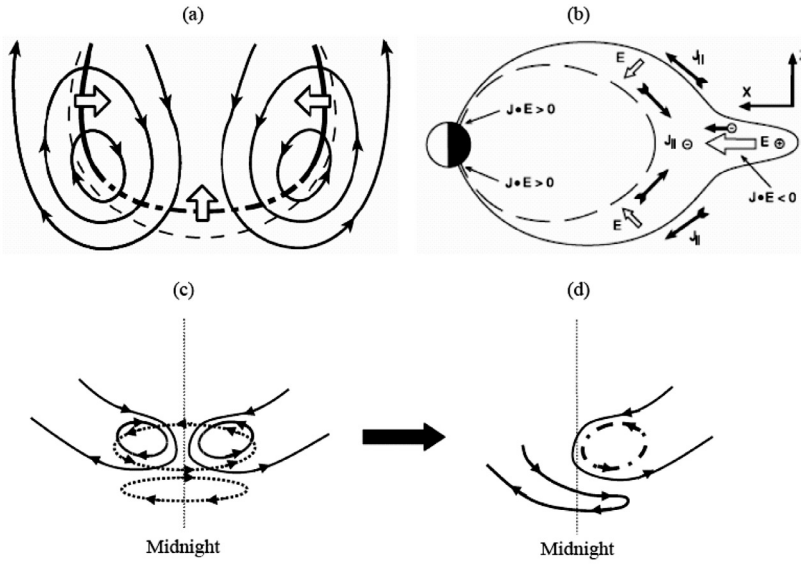

Figure 15. (a) Schematic diagram illustrating the twin-vortex flow pattern generated by the nightside reconnection. The dashed line shows the initial OCFLB; the large arrows show the motion of this boundary under the effect of enhanced nightside reconnection; the heavy lines denote the perturbed OCFLB which is shown solid in the adiaroic portions and dot-dashed in the region of nightside merging gap; the arrowed lines show the plasma streamlines (for details, see *Cowley and Lockwood* [1992]). (b) Schematic of the ''field line slippage'' process in a meridional plane. The dashed and solid curves symbolize the dipole-like and stretched field lines; the hollow arrows denote electric field direction (for details, see *Lui and Kamide* [2003]). (c) The solid curves represent the twin-vortex pattern expected from the night reconnection mechanism; the dotted eclipses represent the convection cells expected from the ''field line slippage'' process. (d) The combined effect of two mechanisms. The high-latitude vortices generated by the above two mechanisms have different rotational senses and tend to cancel each other in the premidnight sector, while in the postmidnight sector they are in the same rotational sense and reinforce each other in the formation of the PoACV (shown in dot-dashed line).

cell was characterized by westward and equatorward flows with much smaller magnitude than the eastward flows in the lower part. This is not fully consistent with a reconnection-driven mechanism, since a reconnection process usually involves an initial flux enhancement first at higher latitudes near the open-closed field line boundary (OCFLB), and the lower-latitude return flows emerges as the secondary stage of evolution. One would expect the initial higher-latitude region to contain the strongest flows and the subsequent lower-latitude region to show weaker flows.

[29] We believe the enhanced eastward flows at lower latitudes are very likely directly related to the substorm-associated process in the central plasma sheet. *Akasofu* [2003] and *Lui and Kamide* [2003] both addressed the importance of the eastward flow enhancement to the substorm EP dynamics. *Akasofu* [2003] suggested that the substorm WEJ is an enhanced Hall current which is by definition antiparallel to the eastward flows. *Lui and Kamide* [2003] proposed a non-MHD mechanism for the generation of the earthward magnetospheric electric field which drives the eastward plasma convection and the MCS. In their scenario, when a substorm EP begins, the magnetic dipolarization rapidly expands rapidly in both the azimuthal and radial directions as the disruption grows from the initial onset region. Since the gyroradius of neutral sheet ions is comparable to or even larger than the current sheet thickness at the late growth phase, the neutral sheet ions are unmagnetized and do not follow the field line motion, but the electrons remain magnetized and therefore tied to the earthward motion of the magnetic field lines. The resulting charge separation between the magnetized electrons and the unmagnetized ions creates both a tailward current and an earthward directed electric field, which is the condition for a dynamo, since $\mathbf{J} \cdot \mathbf{E} < 0$. This dynamo would drive the downward FAC at higher latitudes in the ionosphere and the upward FAC at lower latitudes, constituting the MCS geometry. This non-MHD process is often referred to as ''field line slippage'' and is sketched in Figure 15b. The inward electric field in the equatorial tail maps down to an equatorward field in the auroral ionosphere, resulting in enhanced eastward plasma flows and equatorward Pedersen currents closing the MCS. Anticlockwise and clockwise convection cells appear at higher and lower latitudes, corresponding to the downward and upward FAC regions, respectively.

[30] We suggest that like the coexistence of MCS and zonal SCW currents, the nightside reconnection and the ''field line slippage'' process may both contribute to the development of the PoACV. Their relative contributions may differ between events. The ''field line slippage'' process leads to the enhancement of eastward flows at auroral latitudes, and contributes to those substorms with a more MCS-like current configuration. The nightside reconnection may be responsible for a more SCW-like configuration, as implied from its geometry. Their coexistence may help explain another important feature. From

many available radar convection patterns that we have studied in the premidnight sectors during the substorm EP, we have found that the premidnight clockwise vortex component of the twin-vortex structure that should accompany nightside reconnection is not often visible, or at least is not distinguishable form the preexisting dusk-cell pattern (this statement also applies to the event studied by *Grocott et al.* [2002]). The ''field line slippage'' process and its associated convection vortices should apply in both the premidnight and postmidnight sectors. If one compares the vorticities expected from the reconnection-driven process and from the ''field line slippage'' process (Figure 15c), it is clear that, in the premidnight sector the high-latitude vortices generated by the above two mechanisms have different rotational senses and tend to cancel each other, while in the postmidnight sector they have the same rotational sense and reinforce each other to form a strong PoACV. Also, the enhanced eastward convection associated with the ''field line slippage'' process may facilitate the transport of the newly added closed flux by nightside reconnection to the morning sector; therefore facilitating the formation of the postmidnight flow vortex cycle. The result of these considerations is that the postmidnight vortex should be stronger and, as noticed in our radar observations, is more readily observed than its premidnight counterpart. The remnant part of the evening reconnection cell concatenates with the lower-latitude ''field line slippage'' cell to form a unified flow region with clockwise convection reversal which is associated with the upward FACs. The resulting convection pattern (Figure 15d) agrees well with KY94 model, with the only exception that the lower clockwise cell in KY94 model usually exists not as a separate cell but instead as an eastward extension of the dusk convection cell into the postmidnight sector, characterized by an east-to-west flow reversal in our observations. Such an extension embodies a transition from reconnection-dominated process in the dusk sector to a more directly substorm-associated process, e.g., field-line slippage, at lower latitudes in the near-midnight sector. However, the tail reconnection would still assist the field line slippage in this lower-latitude ''extension cell'' in that both processes convert magnetic energy into particle energy and transport intensified electron fluxes into the near-Earth plasma sheet, which leads to an enhanced auroral electron precipitation and in turn the upward FACs associated with the ''extension cell''. Intense auroral brightenings occur within this ''extension cell'' at places where conditions are stochastically favorable for the magnetospheric-ionospheric feedback instability, which allows for an explosive enhancement of the ionospheric conductances and thus the currents [*Atkinson*, 1970]. The substorm current system inferred from the relative position of the PoACV and bright auroras is thus in general northeast-southwest aligned, but may differ from case to case. The PoACV formation would be greatly facilitated when the auroral breakup happens to occur longitudinally near the postmidnight side of the merging gap, leading to an immediate coupling between the nightside reconnection and ''field line slippage'' process.

[31] In events B and C, for which the subsequent evolution of the PoACV after its initial emergence was available, the PoACV ultimately expanded toward dawn, replacing the preexisting dawn cell and forming a large cell in the postmidnight-early morning sector. The underlying physical mechanism can be understood as follows. When the substorm expands toward the morning sector, the PoACV and its associated downward FAC region will expand as well. When this FAC reaches the lateral edge of the plasma sheet, presumably at the inner edge of the dawnside low-latitude boundary layer, it will connect with the region-1 FAC there (also in general downward) and form a concatenated anticlockwise cell in a substantial portion of the postmidnight-early morning sector. This feature was also seen in the LJ04 event. In that multi-intensification event, we found that such an eastward motion of PoACV after the very first pseudo-breakup represented a transition from an initial MCS-like to a more zonal SCW configuration, the latter becoming the main current system of the final substorm EP onset.

[32] Event D represents a ''frustrated'' evolution of the PoACV. Though we also see the enhancement of eastward convection below $\sim$70° MLAT after the substorm onset, which as we discussed before may be related to the ''field line slippage'' process, and an east-to-west flow reversal region at 65–67° MLAT in the postmidnight sector, there is no clear signature of anticlockwise vortex formation during the event. Near the beginning of the event there is an anticlockwise cell which was located near the pole and in the prenoon sector ($\sim$9 MLT). It is the typical round merging cell seen during dominantly negative IMF By conditions [*Crooker et al.*, 1998; *Watanabe et al.*, 2004]. Between 1148 and 1150 UT there was a transition of the focus of this high-latitude cell, and the focus shifted to the nightside ($\sim$3 MLT) after 1150 UT. This shift indicates that the By-controlled merging process had involved the distant tail lobe, which was in turn arguably associated with the substorm. The round merging cell contained eastward flows in the postmidnight sector, which would have been opposite to the formation of westward flows in the upper part of a developing PoACV. Such a conflict is quite obvious in Figure 14i (1156–1158 UT), when hints of a PoACV seem to appear at 2–3.5 MLT and $\sim$72.5° MLAT. However, this conflict appeared to frustrate the formation of the PoACV. Since on the dawnside a round or ''orange''-shaped convection pattern is common for negative IMF By conditions while a ''banana''-shaped pattern is common for positive By [*Cowley and Lockwood*, 1992], we may speculate that morphologically the formation of a PoACV is preferred under positive IMF By condition but probably suppressed during strong negative By. In the statistical study of global convection pattern during substorms by *Provan et al.* [2004], the statistics are biased to negative IMF By orientation, as stated in their paper. This is possibly one of the reasons why the PoACV is not conspicuous in their results. Also, since the location and formation time of the PoACV, as seen from our events, differ substantially from case to case, its appearance is likely to be obscured by a statistical superposed epoch analysis such as that done by *Provan et al.* [2004].

5. Conclusions

[33] In this paper we have presented a study of postmidnight convection dynamics during the substorm EP, in particular the emergence and subsequent evolution of the postmidnight anticlockwise vortex. The main conclusions follow.

[34] 1. The emergence of the PoACV usually lags the substorm EP onset. The time delay of the formation of the PoACV with respect to the onset depends upon the relative longitudinal separation of the PoACV and the region of brightening aurora. When the PoACV and the initial auroral breakup region have a small longitudinal separation, the PoACV emerges quickly following the onset; otherwise a time delay of a few minutes is required for the establishment of the PoACV. After its emergence the PoACV expands toward dawn and gradually evolves into a large cell in a substantial portion of the postmidnight-early morning sector.

[35] 2. The substorm current system inferred from the relative positions of the PoACV and the auroral brightening region, which are associated with downward and upward FACs, respectively, is in general northeast-southwest aligned. We suggest the actual current system is usually a combination of meridional (MCS) and zonal (SCW) current loops, whose relative importance differs from case to case.

[36] 3. There are two possible generation mechanisms for the PoACV, namely nightside reconnection and/or ''field line slippage'' process associated with the magnetic dipolarization in the central plasma sheet. In particular, the latter mechanism results in the enhancement of eastward convection at auroral latitudes immediately after the substorm EP onset. These two mechanisms lead to the formation of ionospheric vortices that have opposite senses in the premidnight sector but which have the same sense in the postmidnight sector and which therefore reinforce each other in the formation of PoACV. The combined effects of these two mechanisms reproduce both the KY94 model and our observations of a postmidnight anticlockwise cell at higher latitudes, and an east-to-west flow reversal region associated with upward FACs as an extension of the dusk convection cell into the postmidnight sector at lower latitudes.

[37] 4. We found that under negative By-dominated IMF conditions, the round merging cell at very high latitudes appears to conflict with the development of the PoACV. We suggest that strong negative IMF By is unfavorable for the evolution of the PoACV during the substorm EP.

[38] **Acknowledgments.** We acknowledge the national funding agencies of USA, Canada, U.K, and France that support the Northern Hemisphere SuperDARN radars. This research was supported under Natural Sciences and Engineering Research Council of Canada (NSERC) grants. The IMAGE FUV program was supported by NASA. CANOPUS MSP and magnetometer operations were funded by the Canadian Space Agency. The GIMA are operated by the Geophysical Institute of the University of Alaska at Fairbanks. The PBQ magnetometer station is part of the National Geomagnetism Program of the Geomagnetic Laboratory, Geological Survey of Canada. We also thank Bartol Research Institute at the University of Delaware and NOAA National Geophysical Data Center for supplying ACE and GOES satellite data.

[39] Wolfgang Baumjohann thanks Raymond Greenwald and another reviewer for their assistance in evaluating this paper.

References

Akasofu, S.-I. (2003), A source of auroral electrons and the magnetospheric substorm current systems, *J. Geophys. Res.*, *108*(A4), 8006, doi:10.1029/2002JA009547.

Atkinson, G. (1970), Auroral arcs: Result of the Interaction of a Dynamic Magnetosphere with the Ionosphere, *J. Geophys. Res.*, *75*, 4746–4755.

Baker, K. B., and S. Wing (1989), A new magnetic coordinate system for conjugate studies at high latitudes, *J. Geophys. Res.*, *94*, 9139–9143.

Bristow, W. A., A. Otto, and D. Lummerzheim (2001), Substorm convection patterns observed by the Super Dual Auroral Radar Network, *J. Geophys. Res.*, *106*, 24,593–24,609.

Cowley, S. W. H., and M. Lockwood (1992), Excitation and decay of solar wind-driven flows in the magnetosphere-ionosphere system, *Ann. Geophys.*, *10*, 103–115.

Crooker, N. U., J. G. Lyon, and J. A. Fedder (1998), MHD model merging with IMF By: Lobe cells, sunward polar cap convection, and overdraped lobes, *J. Geophys. Res.*, *103*, 9143–9151.

Foster, J. C., and H. B. Vo (2002), Average Characteristics and Activity Dependence of the Subauroral Polarization Stream, *J. Geophys. Res.*, *107*(A12), 1475, doi:10.1029/2002JA009409.

Frey, H. U., S. B. Mende, V. Angelopoulos, and E. F. Donovan (2004), Substorm onset observations by IMAGE-FUV, *J. Geophys. Res.*, *109*, A10304, doi:10.1029/2004JA010607.

Greenwald, R. A., et al. (1995), DARN/SUPERDARN, A global view of the dynamics of high-latitude convection, *Space Sci. Rev.*, *71*, 761–796.

Grocott, A., S. W. H. Cowley, J. B. Sigwarth, J. F. Watermann, and T. K. Yeoman (2002), Excitation of twin-vortex flow in the nightside high-latitude ionosphere during an isolated substorm, *Ann. Geophys.*, *20*, 1577–1601.

Huang, C.-S., J. C. Foster, and J. M. Holt (2001), Westward plasma drift in the midlatitude ionospheric F region in the midnight-dawn sector, *J. Geophys. Res.*, *106*, 30,349–30,362.

Kamide, Y. (1996), The substorm current system: Predicting specific features, *Proceedings of International Conference on Substorms 3*, *ESA SP-389*, pp. 5–10, Eur. Space Agency, Paris.

Kamide, Y., and S. Kokubun (1996), Two-component auroral electrojet: Importance for substorm studies, *J. Geophys. Res.*, *101*, 13,027–13,046.

Kamide, Y., A. D. Richmond, B. A. Emery, C. F. Hutchins, B.-H. Ahn, O. de la Beaujardiere, J. C. Foster, R. A. Heelis, H. W. Kroehl, F. J. Rich, and J. A. Slavin (1994), Ground-based studies of ionospheric convection associated with substorm expansion, *J. Geophys. Res.*, *99*, 19,451–19,466.

Kamide, Y., W. Sun, and S.-I. Akasofu (1996), The average ionospheric electrodynamics for the different substorm phases, *J. Geophys. Res.*, *101*, 99–109.

Kan, J. R., and L. C. Lee (1979), Energy coupling function and solar wind–magnetosphere dynamo, *Geophys. Res. Lett.*, *6*, 577–580.

Khan, H., et al. (2001), Observations of two complete substorm cycles during the Cassini Earth swing-by: Cassini magnetometer data in a global context, *J. Geophys. Res.*, *106*, 30,141–30,175.

Koskinen, H. E. J., and T. I. Pulkkinen (1995), Midnight velocity shear zone and the concept of Harang discontinuity, *J. Geophys. Res.*, *100*, 9539–9547.

Liang, J., G. J. Sofko, E. F. Donovan, M. Watanabe, and R. A. Greenwald (2004a), Convection dynamics and driving mechanism of a small substorm during dominantly IMF By+, Bz+ conditions, *Geophys. Res. Lett.*, *31*, L08803, doi:10.1029/2003GL018878.

Liang, J., G. J. Sofko, and E. F. Donovan (2004b), On the spatial and temporal relationship between auroral intensification and flow enhancement in a pesudosubstorm event, *J. Geophys. Res.*, *109*, A06213, doi:10.1029/2003JA010200.

Liou, K., P. T. Newell, D. G. Sibeck, C.-I. Meng, M. Brittnacher, and G. Parks (2001), Observation of IMF and seasonal effects in the location of auroral substorm onset, *J. Geophys. Res.*, *106*, 5799–5810.

Lui, A. T. Y. (2001), Current controversies in magnetospheric physics, *Rev. Geophys.*, *39*(4), 535–563.

Lui, A. T. Y., and Y. Kamide (2003), A fresh perspective of the substorm current system and its dynamo, *Geophys. Res. Lett.*, *30*(18), 1958, doi:10.1029/2003GL017835.

Lyons, L. R., S. Liu, J. M. Ruohoniemi, S. I. Solovyev, and J. C. Samson (2003), Observations of dayside convection reduction leading to substorm onset, *J. Geophys. Res.*, *108*(A3), 1119, doi:10.1029/2002JA009670.

McPherron, R. L., C. T. Russell, and M. Aubry (1973), Satellite studies of magnetospheric substorms on August 15, 1978, 9, Phenomenological model for substorms, *J. Geophys. Res.*, *78*, 3131–3149.

Opgenoorth, H. J., and R. J. Pellinen (1998), The reaction of the global convection electrojets to the onset and expansion of the substorm current edge, in *Substorms-4*, edited by S. Kokubun and Y. Kamide, p. 663, Terra Sci., Tokyo.

Parkinson, M. L., M. Pinnock, H. Ye, M. R. Hairston, J. C. Devlin, P. L. Dyson, R. J. Morris, and P. Ponomarenko (2003), On the lifetime and extent of an auroral westward flow channel (AWFC) observed during a magnetospheric substorm, *Ann. Geophys.*, *21*, 893–913.

Provan, G., M. Lester, S. B. Mende, and S. E. Milan (2004), Statistical study of high-latitude plasma flow during magnetospheric substorms, *Ann. Geophys.*, *22*, 3607–3624.

Reiff, P. H., and J. L. Burch (1985), IMF By-dependent plasma flow and Birkeland currents in the dayside magnetopause: 2. A global model for northward and southward IMF, *J. Geophys. Res.*, *90*, 1595–1609.

Ruohoniemi, J. M., and K. B. Baker (1998), Large-scale imaging of high-latitude convection with Super Dual Auroral Radar Network HF radar observations, *J. Geophys. Res.*, *103*, 20,797–20,811.

Sofko, G. J., R. A. Greenwald, and W. Bristow (1995), Direct determination of large-scale magnetospheric field-aligned currents with SuperDARN, *Geophys. Res. Lett.*, *22*, 2041–2044.

Troshichev, O. A., V. G. Andrezen, and S. Vennerstroem (1988), Magnetic activity in the Polar Cap - a new index, *Planet. Space Sci.*, *36*, 1095–1102.

Tsyganenko, N. A. (1989), A magnetospheric magnetic field model with a warped tail current sheet, *Planet. Space Sci.*, *37*, 5–20.

Voronkov, I. O. (2005), Near-Earth breakup triggered by the earthward traveling burst flow, *Geophys. Res. Lett.*, *32*, L13107, doi:10.1029/2005GL022983.

Watanabe, M., G. J. Sofko, D. A. Andre, T. Tanaka, and M. R. Hairston (2004), Polar cap bifurcation during steady-state northward interplanetary magnetic field with |BY|∼BZ, *J. Geophys. Res.*, *109*, A01215, doi:10.1029/2003JA009944.

Wild, J. A., and T. K. Yeoman (2000), CUTLASS HF radar observations of high-latitude azimuthally propagating vortical currents in the nightside ionosphere during magnetospheric substorms, *Ann. Geophys.*, *18*, 640–652.

Yeoman, T. K., J. A. Davies, N. M. Wade, G. Provan, and S. E. Milan (2000), Combined CUTLASS, EISCAT and ESR observations of ionospheric plasma flows at the onset of an isolated substorm, *Ann. Geophys.*, *18*, 1073–1087.

H. U. Frey, Space Sciences Laboratory, University of California, Berkeley, 7 Gauss Way, Berkeley, CA 94720-7450, USA.

J. Liang and G. J. Sofko, Institute of Space and Atmospheric Studies, Department of Physics and Engineering Physics, University of Saskatchewan, Saskatoon, Saskatchewan, S7N 5 E2, Canada. (liang@dansas.usask.ca)